The defect-state-assisted enhancement of high harmonic generation in bulk ZnO ⊘

Shuai Xu ; Junhong Yu ✉ ; Chuanbing Ye; Hang Zhang ; Zhan Wang ✉ ; Jianbo Hu ✉

Check for updates

View Online   Export Citation

The defect-state-assisted enhancement of high harmonic generation in bulk ZnO

View Online   Export Citation   CrossMark

Shuai Xu,[1,2,3] (iD) Junhong Yu,[2,a)] (iD) Chuanbing Ye,[2] Hang Zhang,[2,4] (iD) Zhan Wang,[1,3,a)] (iD) and Jianbo Hu[2,4,a)] (iD)

AFFILIATIONS

[1]Institute of Mechanics, Chinese Academy of Sciences, Beijing 100190, China
[2]Laboratory for Shock Wave and Detonation Physics, Institute of Fluid Physics, China Academy of Engineering Physics,
  Mianyang 621900, China
[3]School of Engineering Science, University of Chinese Academy of Sciences, Beijing 100049, China
[4]State Key Laboratory for Environment-Friendly Energy Materials, Southwest University of Science and Technology,
  Mianyang 621010, China

[a)]Authors to whom correspondence should be addressed: jyu012@e.ntu.edu.sg; zwang@imech.ac.cn; and jianbo.hu@caep.cn

ABSTRACT

Optical modulation of high harmonic generation (HHG) at ultrashort timescales is of fundamental interest and central importance for emerging photonic applications. Traditionally, this modulation is realized by injecting incoherent electrons into the conduction band, which can only result in the suppression of HHG intensity. In this work, we have proposed and demonstrated an all-optical route to amplify a specific order of high harmonic generation in (11-20)-cut wurtzite zinc oxide (ZnO) based on the pump-probe configuration. Specifically, intensity enhancement is demonstrated by tuning the wavelength of the generation middle-infrared pulse when the wavelength of HHG matches the energy of a specific defect state. The maximum enhancement factor is observed to be 1.8, while the modulation speed varies with different defect states, which are 0.1 ps for the 5th HHG and 1.5 ps for the 4th HHG. This work might enlighten a new path for ultrafast modulation of HHG in solids for the future development of all-optical devices.

Published under an exclusive license by AIP Publishing. https://doi.org/10.1063/5.0145728

Benefitting from the development of high-intensity lasers, high harmonic generation (HHG) in solids has achieved great success in the last two decades (e.g., the solid-state HHG has been demonstrated for the first time in ZnO with up to the 25th-order HHG,[1] and strong HHG generation induced by elliptically polarized light excitation has been validated in graphene[2]). After demonstrating the generation, how to modulate HHG in solids via external stimuli is becoming the current research focus, considering that modulating HHG would benefit the development of advanced laser sources with a pulse width of attoseconds.[3] Optical modulation is of paramount importance among various proposed HHG modulation mechanisms, which is attributed to the impressive modulation behaviors with a large modulation depth and an ultrafast response time.[4] Furthermore, optical modulation would also help clarify the underlying mechanisms of HHG in solids via perturbation of electronic transitions.[5]

Unfortunately, although outstanding modulation performance of HHG in solids based on optical methods has been demonstrated (e.g., Wang et al. have reported a modulation depth of larger than 90% and a response time of hundreds of picoseconds in ZnO[5]), these proposed optical modulation schemes are all based on the same physical effect: a control pulse is utilized to pump incoherent electrons from the valence band (VB) to the conduction band (CB) and suppress the interband contribution,[5] and, thus, it can only suppress the intensity of HHG. This modulation limitation has enormously hindered the potential applications of HHG in ultrafast optics-related applications since the enhancement of HHG would significantly and immediately impact much research areas in strong-field physics. Therefore, how to enhance HHG in solids by an optical route lies in the main interest of the HHG research community.

Here, the selective enhancement of HHG in the (11–20)-cut single crystal ZnO at the picosecond timescale is demonstrated with the all-optical pump-probe configuration. In our experiment, the wavelength of the middle-infrared (MIR) probe pulse to generate the HHG is varied from 2200 to 2400 nm, and the pump wavelength is fixed at 400 nm. When the HHG wavelength matches the energy of the defect state, a specific order of HHG can be amplified via the stimulated emission process. By changing the time delay between the pump pulse and the MIR pulse, an enhancement factor of 1.8 is observed, while the

modulation speed is determined to be 0.1 ps for the 5th HHG and 1.5 ps for the 4th HHG. The relatively large enhancement factor and the extremely high modulation speed show a quite good modulation performance, which is rarely reported in traditional optical modulation methods. Our works have shown the potential of defects engineering in modulating high harmonic generations, which may enlighten novel photonic applications, e.g., generating intense femtosecond pulses[6] and optimizing the speed of optical switching and communication.[7]

The sample used in our experiments is the (11–20)-cut wurtzite ZnO single crystal, which is prepared by mature hydrothermal growth technique (MTI Co.). First, we have checked the absorption spectrum of the sample, as shown in Fig. 1(a). Based on the spectrum, the bandgap of our sample has been measured to be 3.26 eV (~380 nm). Two defect states have been resolved at the mid-gap position, which can be seen more clearly in the inset of Fig. 1(a). Based on the aforementioned results, the energy band of our sample is illustrated in Fig. 1(b), matching well with our previous work[8] or other works about ZnO.[9] The native ZnO defects are donor-type defects (i.e., the carriers are electrons), which are associated with the crystalline imperfection due to point defects.[9,10]

The experimental setup is shown in Fig. 1(c). Femtosecond laser pulses from a regenerative amplified Ti:sapphire system (Spectra-Physics, central wavelength: 800 nm, pulse duration: 50 fs, and the repetition rate: 1 kHz) are used as the laser source. A TOPAS laser system (an optical parametric amplifier, Spectra-Physics) is utilized to convert the 800 nm pulses to the MIR pulse with a wavelength ranging from 2200 to 2400 nm, which is used to generate the HHG with a fixed fluence of 400 mJ/cm^2. The HHG spectra are detected with a commercial

spectrometer (Ocean Optics). Another 800 nm pulse from the femtosecond laser source is frequency-doubled by a BBO crystal (barium metaborate) to serve as the pump beam and then focused on the ZnO crystal at the same position as the MIR beam. The pulse duration of the pump is 70 fs, and the pulse duration of the MIR is about 150 fs. The bandwidth of the MIR measured in the experiment is about 30 nm (the full width at half maximum, FWHM). The polarization of the pump beam is set parallel to the polarization of the MIR beam using a half-wave plate, for the purpose of obtaining a strong optical response. The time separation between the pump and MIR beams is adjusted by a delay line stage, which is synchronized to the spectrometer by a computer. All the experiments are done at ambient pressure and room temperature.

The HHG spectra of the sample generated by the MIR pulse with the wavelength of 2310 nm are shown in Fig. 1(d). The 4th HHG (HH4) to the 9th HHG (HH9) spectra can be clearly observed, and no physical damage to our sample is identified during the measurement. It is worth noting that the (11–20)-cut ZnO is anisotropic, and different MIR polarizations would induce different HHG spectra. In this experiment, the MIR polarizations are either parallel or perpendicular to the c-axis (i.e., the (0001)-axis). When the MIR polarization is perpendicular to the c-axis, the even-order HHG is suppressed, and only HH4 is observed. While for the parallel condition, the even-order HHG becomes much stronger. Specifically, the intensity of HH4 is above the instrument measurement range with this integration time setup. Our HHG spectra results are consistent with previous works.[12]

Then, a pump pulse with a wavelength of 400 nm is used to modulate the HHG spectra. The polarizations of the MIR pulse and the
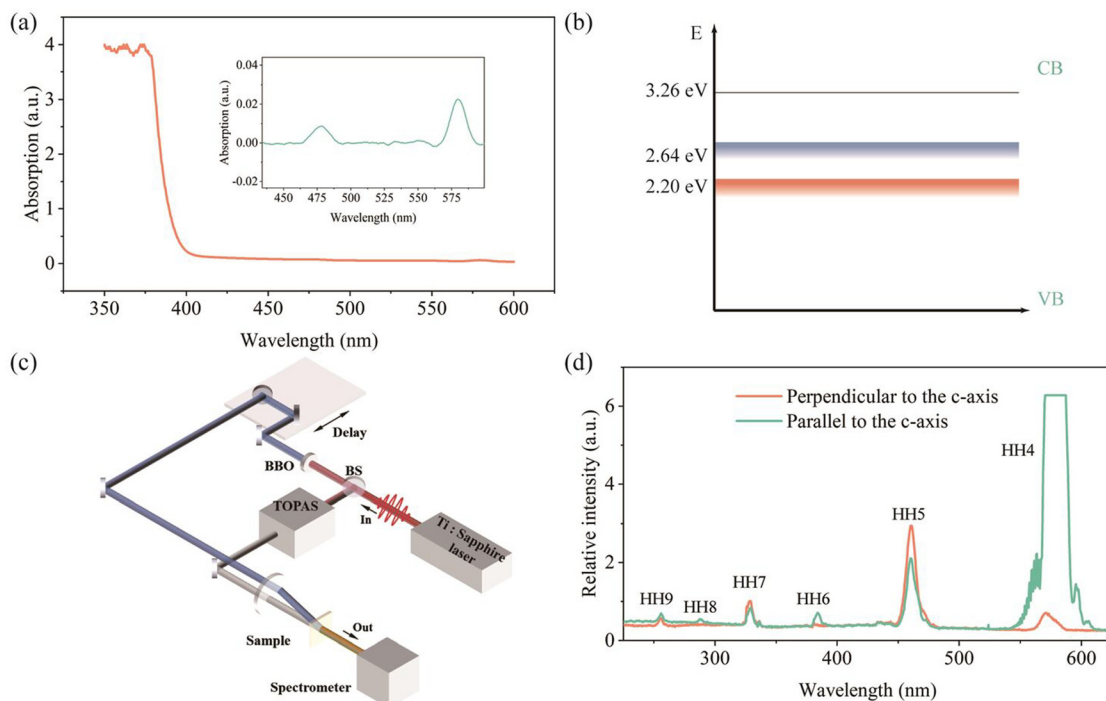

FIG. 1. (a) The absorption spectrum of the ZnO sample. The inset shows two defect-state-related absorption features. (b) The energy band sketch map based on the absorption spectrum. (c) A schematic of the experimental setup. (d) HHG spectra of the (11-20)-cut ZnO excited by the 2310 nm MIR pulse with two different polarizations.

pump pulse are perpendicular to the c-axis of our sample. The modulation result is shown in Fig. 2(a), and the detailed dynamics of HH4, HH5, and HH7 is demonstrated in Fig. 2(b). When the delay is positive (i.e., the pump pulse arrives earlier than the MIR pulse), the intensity of HHG is modulated with different performances for different-order HHG. For HH4, HH7, or other orders not shown in this figure, the intensity would be temporally suppressed, which is consistent with the results in earlier works.[5,11,13,14] Based on the conclusion of the previous works,[11] the HHG suppression process should be related to the electron excitation process from the VB to the CB. After the excitation process, the electrons at CB decay to VB, thus inducing a recovery process. However, it is pretty abnormal for HH5, with the intensity larger than the initial value with an enhancement factor of 1.8. The unusual dynamics of HH5 is inconsistent with the reported suppression behavior, requiring further investigations. Also it is worth noting that the modulation speed in this experiment is extremely fast, determined to be 0.1 ps. For the traditional method based on electron injection into the conduction band, the modulation speeds are usually several picoseconds or even longer. In addition to the aforementioned phenomena, it is also observed that the spectral shape of HH5 splits in the delay time range of 0.5–1.5 ps in Fig. 2(a). This phenomenon has been systematically investigated in our previous HHG modulation work[11] and can be attributed to the coherent mixing-frequency process. The nonlinear frequency mixing process occurs efficiently with a threshold; therefore, the high-intensity part of HH5 will be suppressed, which makes the spectra look like "splitting."

The dynamics of HH5 with a delay time around zero is shown in Fig. 2(c) for several MIR wavelengths. It is found that the enhancement is quite sensitive to the MIR wavelength. For 2310 nm, the intensity is enhanced, while for 2290 or 2330 nm, we can only observe the suppression effect. Meanwhile, we have also checked the pump fluence-dependent HH5 intensity when the MIR wavelength is fixed at 2310 nm, as shown in Fig. 2(d). Surprisingly, we observed no monotonous trend in the enhancement factor with an increase in pump fluence (i.e., the largest enhancement factor of 1.8 is observed with a fluence of 16 mJ/cm^2, even stronger than the 24 mJ/cm^2 excitation). These results cannot be interpreted by the traditional HHG modulation mechanisms[5] and indicate a complex and competing mechanism.

As shown in Figs. 1(a) and 1(d), the wavelength of the enhanced HH5 is 462 nm (2.68 eV), quite close to the energy of the defect state at 2.64 eV (please note that the slight energy difference between HH5 and the defect state can be possibly attributed to the quiver energy induced resonance tuning effect[1,15]). Thus, a rational assumption is that the enhancement is associated with the specific defect state. To verify this assumption, we have tried to explore the enhancement of other-order HHG, and the HH4 intensity has been successfully enhanced. In this experiment, the MIR polarization is set parallel to the c-axis; thus, we can easily detect the intensity change of HH4 because HH4 is relatively strong at this condition. As shown in Fig. 3(a), the enhancement of HH4 is obtained when the MIR wavelength is 2240 nm. Meanwhile, the HH5 shows almost no change with different pump fluences, which can be seen in the inset. Similar to the last case, the enhancement is also quite sensitive to the MIR
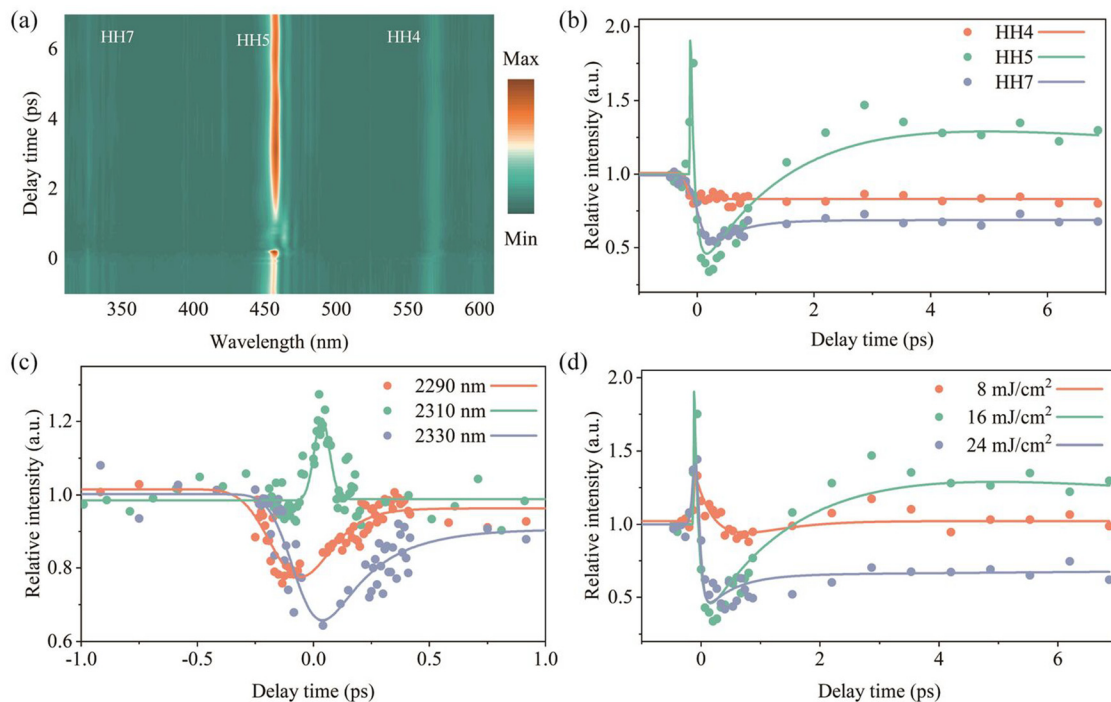
FIG. 2. (a) and (b) The HHG spectra as a function of the delay time. The whole intensity spectrum is shown in (a), and the relative intensities of HH4, HH5, and HH7 are shown in (b). The HH5 is obviously enhanced by a factor of 1.8. (c) The HH5 dynamics at the region near the zero delay with different MIR wavelengths of 2290, 2310, and 2330 nm. HH5 is enhanced only for the 2310 nm condition. (d) The HH5 dynamics with different pump fluences. The maximal enhancement factor is achieved at 16 mJ/cm^2.

FIG. 3. (a) The HHG spectra with pump or without pump when the MIR wavelength is 2240 nm. The inset shows the HH5 spectrum. The HH4 is enhanced obviously, while the HH5 has almost no difference. (b) The relative intensity of HH4 as a function of the delay time when the MIR wavelength is 2240 nm.

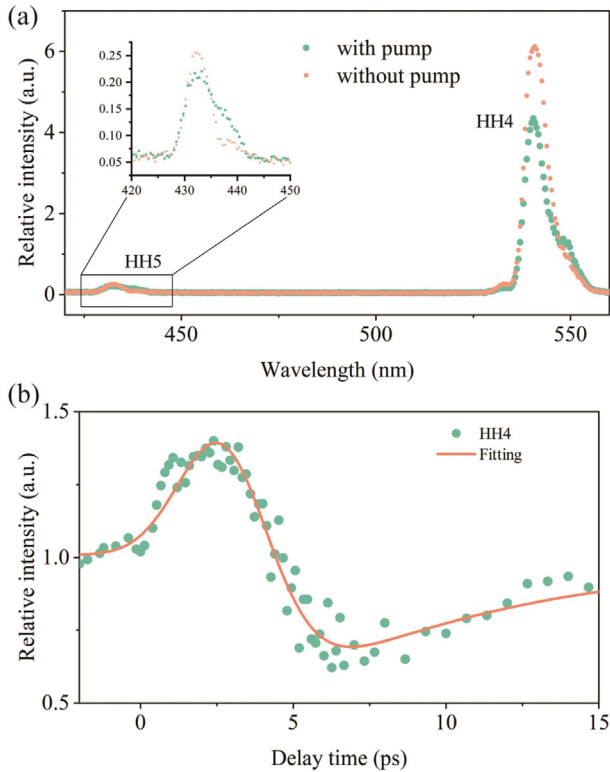wavelength, and it cannot be observed for 2220 or 2260 nm. The results have shown strong evidence to support our assumption because the wavelength of HH4 is detected to be 548 nm (2.26 eV), quite close to the defect state at 2.20 eV.

As shown in Fig. 3(b), the HH4 dynamics has also been measured, showing different dynamic curve compared to the HH5

dynamics in Fig. 2. For HH5, the enhancement near the zero delays can only last for 0.2 ps (i.e., the half of which is the modulation speed), while 3 ps for HH4. The significant time difference indicates that the enhancement for HH4 and HH5 should originate in different states. It is rational since we attribute the different dynamics to the different defect states.

Based on the aforementioned results, we have proposed an assumption to explain the HHG enhancement phenomenon. As shown in Fig. 4, we take the enhancement of HH5 as an example and draw a sketch map to illustrate the proposed mechanisms. Generally, two conflicting mechanisms would participate in our experiments, which have inverse effects on the intensity of HHG. First, we would mention the three-step model in HHG: (i) electron tunneling excitation, (ii) electron or hole acceleration, and (iii) electron–hole recombination.[16–18] With a pre-excitation pump pulse, electrons in the VB would be excited to the CB, which should suppress step iii (i.e., the interband contribution to HHG). Thus, the intensity of HHG is suppressed, which has been widely observed in previous works.[5,11–13] In these experiments, the electrons in CB should be the dominant mechanism, and it is also one ongoing process in our work. However, in our hypothesis, there should be another process with the inverse effect: the pre-excitation pump pulse would also excite electrons to the defect state. It is worth noting that the electrons in defect states should come from two channels: (i) electrons can be directly excited to the defect level from the lower part of the valence band; (ii) electrons in the conduction band can be trapped by the defect level before they recombine to the valence band. If the wavelength of HH5 is quite close to the energy of the defect state (2.64 eV), the electrons in the defect state will participate in the HHG generation process. The HH5 photons generated by MIR would induce the radiative recombination of electrons from the defect state to VB, similar to the three-energy level stimulated emission process.[19] As a result of this process, additional HH5 photons are radiated, and the enhancement of HH5 is achieved. Please note that the wavelength of HHG is the key to the enhancement mechanism. The ultra-narrow bandwidth of the enhancement is due to the energy distribution of the discrete defect state. As shown in Fig. 1(a), the density of states of two discrete defect states is restricted in a narrow wavelength range. If the wavelength of HH5 is shifted from the energy of the defect state, the stimulated emission would disappear,
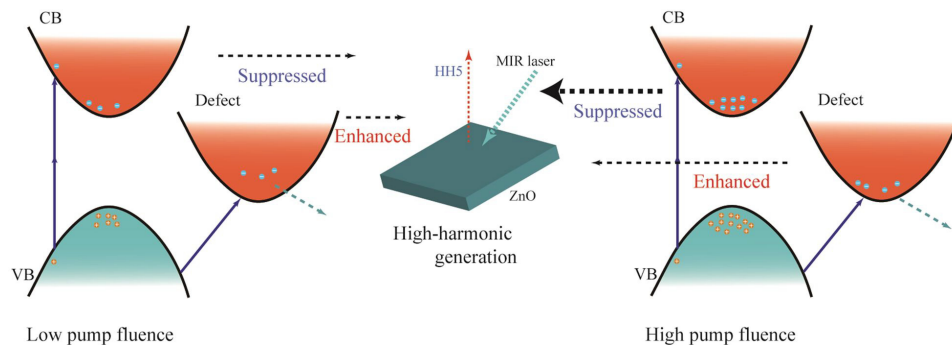
FIG. 4. The sketch map of the amplified HHG mechanisms. The pump pulse would inject electrons into defect states and CB, resulting in two competition HHG modulation mechanisms (the left panel). The electrons in defect states would enhance the specific order of HHG via the stimulated emission, while the electrons in CB would suppress all orders of HHG via incoherent electron injection. Higher pump fluence would increase the populations of electrons in both defect and CB. However, if the electron population in defect states is saturated, higher pump fluence would not induce large enhancement (the right panel).

and the radiation from the defect state to VB cannot enhance the HH5 intensity anymore. The suppression effect would be the dominant mechanism for this condition, and no enhancement would be observed. The earlier is the interpretation of the HH5 enhancement, which is also applicable to the enhanced HH4 in Fig. 3. The HH4 enhancement phenomenon should be associated with the defect state at 2.20 eV.

Furthermore, the unusual phenomenon in Fig. 2(d) can be interpreted using the above-proposed mechanisms. In principle, the population of electrons excited to the CB, and the defect state would be larger with higher pump fluence. Based on our hypothesis, these two increased populations of electrons would have opposite influences on the intensity of HHG, inducing the complex phenomenon in Fig. 2(d). On the one hand, more electrons in the CB would suppress the intensity of HHG by decreasing the interband contribution. On the other hand, more electrons in the defect state could radiate more HH5 photons. For ease of understanding, a brief description of these two competitive mechanisms has been shown in Fig. 4. When the pump fluence is 8 mJ/cm^2 in Fig. 2(d), few electrons are excited to the defect state, resulting in weak radiation from the defect state to the VB. Thus, the enhancement factor is only 1.3 for low pump fluence. However, the enhancement factor is still relatively small (1.4) for high pump fluence (24 mJ/cm^2). This can also be interpreted by our hypothesis, shown in the right panel of Fig. 4. For this condition, the population of electrons in the defect state would be saturated, and the enhancement effect is independent of the further increase in pump fluence. On the other hand, a higher pump fluence would continuously inject electrons into CB and make the suppression effect larger. Therefore, a higher pump fluence may not ensure a larger enhancement effect, which is verified in Fig. 2(d) (i.e., the enhancement of 16 mJ/cm^2 is larger than that of 24 mJ/cm^2). Based on the aforementioned discussion, an optimized pump fluence is required to achieve an outstanding performance of HHG enhancement.

Based on the aforementioned conclusions, the increase/decrease/increase shape for HH5 in Fig. 2(b) can also be explained. The first increase trend is because of the stimulated emission enhancement. In this condition, there are increasing electron populations both in the conduction band and defect state, and electrons in the defect state would enhance HHG via the stimulated emission process. After this trend, the intensity of HHG would decrease because of the decrease in electron population in the defect state, attributed to the ultrafast lifetime of the stimulated emission process. As a result, incoherent electrons in the conduction band would dominate the modulation process of HHG after the stimulated emission process, leading to a decreased trend in the HHG intensity. Finally, the HHG intensity would increase again because of the interband recombinations of the electrons. The population of the electrons in the conduction band would decrease gradually, and, thus, the suppression of HHG would also become weaker.

In our works, all dynamic curves are fitted by the following exponential function convoluted with a Gaussian instrument response,[11] shown as solid lines in Figs. 2(b)–2(d) and 3(b):

$$I = A_1 \cdot erf\left(\frac{t - t_0}{\tau_0} - \frac{\tau_0}{2\tau_1}\right)\exp\left(-\frac{t}{\tau_1}\right)$$
$$+ A_2 \cdot erf\left(\frac{t - t_0}{\tau_0} - \frac{\tau_0}{2\tau_2}\right)\exp\left(-\frac{t}{\tau_2}\right)$$
$$+ A_3 \cdot erf\left(\frac{t - t_0}{\tau_0} - \frac{\tau_0}{2\tau_3}\right)\exp\left(-\frac{t}{\tau_3}\right), \tag{1}$$

where τ_1, τ_2, and τ_3 are the lifetime constants for different processes, while τ_0 is the pulse width of the pump pulse (i.e., the instrument response). The coefficients A_1, A_2, and A_3 are the amplitudes of each process. When the coefficient is positive, it is an enhancement process, while it is a suppression process for the negative coefficient. All fitting parameters are provided in the supplementary material as Table S1.

In principle, all the exponential terms of the normal HHG modulation are decaying,[11,13] which would indicate the interband transition process from the CB to the VB. For our HHG enhancement data, the exponential terms would be a growing term and two decaying terms, corresponding to the two competitive mechanisms. Based on the aforementioned discussion, the growing term indicates the electron dynamics of defect states, while the decaying terms reflect the dynamics of CB. Thus, we can directly obtain the dynamics of the defect state using the HHG enhancement experimental data. According to the fitting parameters, the growing lifetimes are 0.1 and 2 ps for the 2.64 and 2.20 eV defect states, respectively. It is worth noting that the dynamics of HH5 and HH4 is quite different in Figs. 2 and 3, showing the potential to detect the defect state dynamics.

In conclusion, we have generated HHG in (11–20)-cut ZnO with MIR excitations and modulated it using a 400 nm pump pulse. In our experiment, the specific order of HHG has been enhanced using the all-optical pump-probe method. An enhancement factor of 1.8 has been obtained by varying the time delay between the pump pulse and the MIR pulse. The enhancement can be achieved when the HHG wavelength matches the energy of a specific defect state, which is attributed to the stimulated emission. Also, we have found that the enhancement performances are quite different for different-order HHG. Specifically, the modulation speed is determined to be 0.1 ps for the 5th HHG and 1.5 ps for the 4th HHG. The significant difference has shown the potential to determine the carrier dynamics of the specific defect state. Our work has enriched the optical modulation scheme of HHG in solids.

See the supplementary material for fitting parameters to fit all dynamic curves shown in Figs. 2(b)–2(d), and 3(b).

AUTHOR DECLARATIONS
Conflict of Interest

The authors have no conflicts to disclose.

Author Contributions

Shuai Xu: Formal analysis (lead); Investigation (lead); Visualization (lead); Writing – original draft (lead). **Junhong Yu:** Data curation (lead); Formal analysis (equal); Investigation (equal); Project administration (equal); Supervision (supporting); Validation (lead); Visualization (equal); Writing – original draft (equal). **Chuanbing Ye:** Investigation (supporting); Methodology (supporting); Writing – review & editing (supporting). **Hang Zhang:** Investigation (supporting); Methodology (equal); Validation (equal); Writing – review &

DATA AVAILABILITY

The data that support the findings of this study are available from the corresponding authors upon reasonable request.

REFERENCES

[1] S. Ghimire, A. D. Dichiara, E. Sistrunk, P. Agostini, L. F. Dimauro, and D. A. Reis, "Observation of high-order harmonic generation in a bulk crystal," Nat. Phys. **7**, 138–141 (2011).

[2] N. Yoshikawa, T. Tamaya, and K. Tanaka, "High-harmonic generation in graphene enhanced by elliptically polarized light excitation," Science **356**, 736–738 (2017).

[3] Z. N. Zeng, Y. H. Zheng, Y. Cheng, R. X. Li, and Z. Z. Xu, "Attosecond pulse generation driven by a synthesized laser field with two pulses of controlled related phase," J. Phys. B: At., Mol. Opt. Phys. **45**, 074004 (2012).

[4] Y. Cheng, H. Hong, H. Zhao, C. C. Wu, Y. Pan, C. Liu, Y. G. Zuo, Z. H. Zhang, J. Xie, J. H. Wang, D. P. Yu, Y. Ye, S. Meng, and K. H. Liu, "Ultrafast optical modulation of harmonic generation in two-dimensional materials," Nano Lett. **20**, 8053–8058 (2020).

[5] Z. Wang, H. Park, Y. H. Lai, J. L. Xu, C. I. Blaga, F. Y. Yang, P. Agostini, and L. F. DiMauro, "The roles of photo-carrier doping and driving wavelength in high harmonic generation from a semiconductor," Nat. Commun. **8**, 1686 (2017).

[6] A. R. A. Ganeev, T. Witting, C. Hutchison, F. Frank, M. Tudorovskaya, M. Lein, W. A. Okell, A. Zaïr, J. P. Marangos, and J. W. G. Tisch, "Isolated sub-fs XUV pulse generation in Mn plasma ablation," Opt. Express **20**, 25239–25248 (2012).

[7] W. Li, B. G. Chen, C. Meng, W. Fang, Y. Xiao, X. Y. Li, Z. F. Hu, Y. X. Xu, L. M. Tong, H. Q. Wang, W. T. Liu, J. M. Bao, and Y. R. Shen, "Ultrafast all-optical graphene modulator," Nano Lett. **14**, 955–959 (2014).

[8] C. Gu, H. Zhang, Y. G. Liu, J. H. Yu, J. H. Pan, G. Q. Luo, Q. Shen, J. Tang, and J. B. Hu, "Time-domain observation of spectral diffusion in defective ZnO," ACS Omega **6**, 15442–15447 (2021).

[9] L. Foglia, S. Vempati, B. T. Bonkano, L. Gierster, M. Wolf, S. Sadofev, and J. Stahler, "Revealing the competing contributions of charge carriers, excitons, and defects to the non-equilibrium optical properties of ZnO," Struct. Dyn. **6**, 034501 (2019).

[10] M. D. McCluskey and S. J. Jokela, "Defects in ZnO," J. Appl. Phys. **106**, 071101 (2009).

[11] S. Xu, H. Zhang, J. H. Yu, Y. D. Han, Z. Wang, and J. B. Hu, "Ultrafast modulation of high harmonic generation in bulk ZnO single crystal," Opt. Express **30**, 41350–41358 (2022).

[12] S. Gholam-Mirzaei, J. Beetar, and M. Chini, "High harmonic generation in ZnO with a high-power mid-IR OPA," Appl. Phys. Lett. **110**, 061101 (2017).

[13] M. R. Bionta, E. Haddad, A. Leblanc, V. Gruson, P. Lassonde, H. Ibrahim, J. Chaillou, N. Emond, M. R. Otto, A. Jimenez-Galan, R. E. F. Silva, M. Ivanov, B. J. Siwick, M. Chaker, and F. Legare, "Tracking ultrafast solid-state dynamics using high harmonic spectroscopy," Phys. Rev. Res. **3**, 023250 (2021).

[14] C. Heide, Y. Kobayashi, A. C. Johnson, F. Liu, T. F. Heinz, D. A. Reis, and S. Ghimire, "Probing electron-hole coherence in strongly driven 2D materials using high-harmonic generation," Optica **9**, 512–516 (2022).

[15] K. J. Schafer, B. Yang, L. F. DiMauro, and K. C. Kulander, "Above threshold ionization beyond the high harmonic cutoff," Phys. Rev. Lett. **70**, 1599–1602 (1993).

[16] M. Lewenstein, P. Balcou, M. Y. Ivanov, A. L'Huillier, and P. B. Corkum, "Theory of high-harmonic generation by low-frequency laser fields," Phys. Rev. A **49**, 2117 (1994).

[17] C. Yu, S. C. Jiang, and R. F. Lu, "High order harmonic generation in solids: A review on recent numerical methods," Adv. Phys.: X **4**, 1562982 (2019).

[18] L. Yue and M. B. Gaarde, "Imperfect recollisions in high-harmonic generation in solids," Phys. Rev. Lett. **124**, 153204 (2020).

[19] E. A. Prasetyanto, H. S. Wasisto, and D. Septiadi, "Cellular lasers for cell imaging and biosensing," Acta Biomater. **143**, 39–51 (2022).